

A hydro-mechanical elastoplastic model for unsaturated soils under isotropic loading conditions

H. Ghasemzadeh, S.A. Ghoreishian Amiri *

Faculty of Civil Engineering, K.N. Toosi University of Technology, Tehran, Iran



ARTICLE INFO

Article history:

Received 24 December 2011

Received in revised form 31 January 2013

Accepted 7 February 2013

Keywords:

Elastoplastic behavior

Unsaturated soil

Hydro-mechanical coupling

Collapsible soil

Expansive soil

ABSTRACT

This paper presents an elastoplastic constitutive model for the coupling of hydraulic and stress-strain behavior of unsaturated soils under isotropic loading conditions. The proposed model is capable of considering the influence of irrecoverable changes in water volume fraction on stress-strain behavior and plastic strain on hydraulic behavior. Bounding surface and subloading surface plasticity frameworks are employed to describe hydraulic and mechanical behavior, respectively. The appropriate coupled hardening rules are introduced to fully describe the coupling effects between hydraulic and stress-strain behavior. Model predictions for unsaturated highly expansive and collapsible soils are compared with test data, and reasonable agreement is achieved.

© 2013 Elsevier Ltd. All rights reserved.

1. Introduction

The constitutive modeling of unsaturated soils and rocks has been closely linked with efforts to identify the relevant stress variables describing the behavior of unsaturated soils (e.g. [1–3]). Three types of approaches are commonly used to simulate unsaturated soil behavior: the generalized effective stress concept, two stress-state variables, and the theory of mixture.

The so-called generalized effective stress theory has been widely used in the literature to describe the behavior of unsaturated soils. Effective stress-based models generally use Bishop's formula [4]. However, numerous researchers (e.g. [3,5–11]) have questioned the validity of Bishop's effective stress formula for unsaturated soils. In contrast, several investigators (e.g. [12–19]) have proven that Bishop's effective stress formula, when used within a proper elastoplastic framework, can readily describe the complex behavior of unsaturated soils, such as the phenomenon of collapse upon wetting.

In the last two decades, two stress-state variables have been increasingly used to describe the hydro-mechanical behavior of unsaturated soils (e.g. [20–25]). Several aspects of the hydro-mechanical behavior of unsaturated soils can be successfully simulated by adopting two stress-state variables [26]. Commonly, net stress and matric suction are selected as the stress-state variables in these types of models (e.g. [20]).

Using experiments, Wheeler [27], Sharma [28] and Sun et al. [29] demonstrated that using net stress and matric suction as the stress-state variables could not simulate the influence of water volume fraction (or degree of saturation) on stress-strain behavior. Moreover, these types of models could not capture the influence on variations in water volume fraction of the volumetric strains. In recent years, several researchers have started to propose elastoplastic constitutive models for considering the effects of deformation on soil water characteristic curves (SWCCs) and coupling effects on the reverse direction [29–35].

Wheeler et al. [30] proposed an initial framework for simulating the influence of degree of saturation on mechanical behavior and the influence of volumetric strain on hydraulic behavior. They employed Bishop's effective stress and modified suction as the stress-state variables. However, the model suffers from some particular weaknesses due to the simple mathematical expressions within the constitutive equations. For instance, the assumed hysteresis in this model for SWCCs is too simple to represent the experimentally observed curves [33]. Fig. 1 shows the schematic of water retention behavior assumed by Wheeler et al. [30].

Sheng et al. [31] proposed that applying Bishop's effective stress and suction (instead of modified suction) as the stress-state variables were sufficient for deriving constitutive equations for considering the coupling effects of mechanical behavior and degree of saturation. Applying this set of stress-state variables, Sun et al. [32] presented an elastoplastic model for the hydro-mechanical behavior of unsaturated soils. However, it seems that they tended to accentuate the influence of the hydraulic behavior on the

* Corresponding author. Tel.: +98 9111135424; fax: +98 2188779476.

E-mail address: sa_ghoreishian@dena.kntu.ac.ir (S.A. Ghoreishian Amiri).

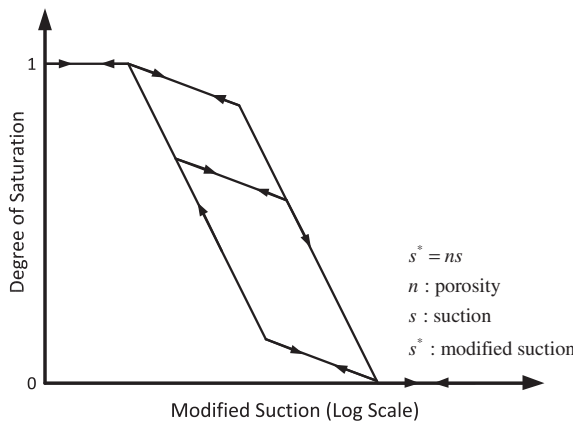


Fig. 1. Water retention behavior of the model proposed by Wheeler et al. [30].

mechanical behavior, placing less emphasis on the influence of mechanical behavior on hydraulic behavior [36].

Muraleetharan et al. [33] combined the theory of mixture with interface and the continuum theory of plasticity to improve Wheeler et al.'s [30] framework. Using thermodynamics, they demonstrated that the conjugate stress variables with plastic strain and the irrecoverable part of the water volume fraction are intergranular stress tensor (as later defined) and matric suction, respectively. They proceeded to use intergranular stress tensor and matric suction as the stress-state variables. They employed a bounding surface plasticity framework [37,38] to simulate hysteresis in SWCCs. Although this model is capable of simulating problems that involve multiple cycles of wetting and drying, it cannot properly simulate the multiple cycles of mechanical loading and unloading. The mechanical constitutive equations of this model are based on the assumption that the interior of the yield surface is a purely elastic domain. This idealized assumption causes the model to predict purely elastic strains for cyclic loading paths inside the yield surface. Therefore, it cannot predict the cyclic loading behavior of materials, for example, for loading paths with constant stress amplitude. It seems that is why they just presented qualitative results for the problems involve multiple cycles of mechanical loading and unloading. Furthermore, the coupled movement of the mean wetting and drying curves due to the occurrence of plastic deformation is not considered in this model (also see Wheeler et al. [30]).

Another approach for modeling hydro-mechanical behavior of unsaturated soils is using the continuum theory of mixture (e.g. [14,39]). This type of approach generally provides more consistent description of various coupling mechanisms between the hydraulic and mechanical behavior of unsaturated soils. One of the difficulties in utilizing the theory of mixture is that since some state variables cannot be directly measured through experiments, phenomenological relations must be introduced to characterize these variables [33].

In this paper, as the first step, a coupled hydro-mechanical model of unsaturated soils under isotropic loading conditions is introduced in the framework of two stress-state variables. Similar to Muraleetharan et al. [33], intergranular stress and matric suction are selected as the two stress-state variables. The main purpose of this paper is to present a more realistic model for simulating the coupled hydro-mechanical behavior of unsaturated soils. In the proposed model, more efficient constitutive equations and coupled hardening rules are introduced to improve the framework proposed by Wheeler et al. [30] and developed by Muraleetharan et al. [33]. The proposed model is capable of considering the influence of the water volume fraction on mechanical behavior,

such as irreversible compression during the drying path that do not exceed the maximum value of suction previously experienced by the soil and coupling effects on the reverse direction as well as the variation of the water volume fraction due to mechanical loading or unloading. These capabilities are examined by comparing the model predictions with experiments.

It is worth noting, however, that while the applicability of the present model is limited to isotropic loading conditions, the model provides a very useful framework for future studies to develop a constitutive model for general loading conditions.

Note that throughout this paper, compression stress and strain are assumed to be positive.

2. Coupled elastoplastic framework

It is assumed that the water volume fraction increment (dn_w), such as the strain increment ($d\varepsilon$), is additively decomposed into elastic and plastic parts:

$$d\varepsilon = d\varepsilon^e + d\varepsilon^p \quad (1)$$

$$dn_w = dn_w^p + dn_w^e \quad (2)$$

where the water volume fraction is defined as the fraction of the total volume of soil that is occupied by water.

The appropriate selection of conjugated stress and strain variables is essential for the construction of constitutive models for unsaturated soil. Wei [40] showed that plastic deformation and capillary hysteresis are restricted by the following dissipation inequalities:

$$\sigma^* : d\varepsilon^p + q_k \cdot d\alpha_k \geq 0 \quad (3)$$

$$-s \cdot dn_w^p + \gamma_l \cdot dv_l \geq 0 \quad (4)$$

where s is the matric suction; α_k is a set of internal variables characterizing the hardening response of the material; v_l is a set of internal variables characterizing the capillary hysteresis effects; q_k and γ_l are internal forces associated with α_k and v_l , respectively. σ^* is the intergranular stress tensor, which is defined as:

$$\sigma^* = \sigma_{net} + n_w s \mathbf{I} \quad (5)$$

where \mathbf{I} is the unit tensor, and σ_{net} is net stress tensor. Eqs. (3) and (4) imply that the intergranular stress tensor (σ^*), the matric suction (s), the plastic deformation ($d\varepsilon^p$) and the irrecoverable part of the volume fraction (dn_w^p) are the conjugated stress-strain variables, which are thermodynamically consistent. These stress-strain variables were successfully used by Muraleetharan et al. [33].

The intergranular stress tensor (σ^*) equals Bishop's effective stress by setting $\chi = n_w$ for unsaturated and $\chi = 1$ for saturated conditions. It means that a switch is required so that when the value of suction is greater than zero, then $\chi = n_w$, whereas when the value of suction is equal to zero, then $\chi = 1$. Consequently, the intergranular stress tensor becomes Terzaghi's effective stress in a fully saturated condition, and thus, the transition between saturated and unsaturated conditions can be performed without any problem [33]. It is worth noting, since the value of suction at the moment of transition between saturated and unsaturated conditions is equal to zero, the effective stress and intergranular stress will not be affected by the value of χ . In other words, although at the moment of transition the value of χ is defined discontinuously the intergranular stress tensor treats continuously.

As the proposed model is focused on isotropic loading conditions, the intergranular mean stress (p^*) and matric suction (s) are considered the stress variables. The volumetric strain (ε_v) and water volume fraction (n_w) are selected as the strain variables.

The process of slippage, widening and closing between granular medium particles is associated with a loading collapse (LC) yield surface. For isotropic loading condition, this simplifies to an LC yield curve in the $p^*:s$ plane. Based on the fact that the presence of meniscus water is more important for the overall stability of the soil skeleton than the value of suction, Wheeler et al. [30] showed that the LC yield curve could be assumed a straight line in the effective mean stress and modified suction plane. It is worth noting that their argument was presented based on inter-particle normal forces and suction, and thus, it can be used in our study. Following this line of discussion, the LC yield curve is considered a straight line in the $p^*:s$ plane. The subloading surface plasticity framework [41,42], with some simplification, is adopted for simulating mechanical behavior. The subloading surface plasticity framework fulfills all the fundamental and mechanical requirements of developing stress-strain constitutive equations: the continuity condition, the smoothness condition and the work rate-stiffness relaxation [43]. Thus, it is not necessary to judge the fulfillment of the yield condition. Moreover, by the use of a controlling function within the model, it could automatically pull back the stress point into the normal yield surface even if it goes out from the surface [44]. Consequently, a rough numerical calculation with large loading steps is allowed in subloading surface models. Furthermore, since there is no purely elastic domain in the selected framework, the proposed model could simulate elastoplastic deformation even for the cyclic loading paths with constant amplitude. In relation to the selected framework, the LC yield curve is renamed the *LC normal yield curve* in the proposed model.

Irrecoverable change of n_w occurs in both wetting and drying processes. The suction increase (SI) yield curve and suction decrease (SD) yield curve can control the plastic change of n_w in drying and wetting paths, respectively. The shape of SI and SD yield curves is considered a straight line in the $p^*:s$ plane [33]. The evolution of the irrecoverable part of the water volume fraction and hysteresis (SWCCs) could be captured within an appropriate elastoplastic framework. The bounding surface plasticity was previously employed successfully for simulating hydraulic behavior during wetting and drying cycles by Li [45], Liu and Muratheelaran [46], Kohgo [47] and Muratheelaran et al. [33]. Furthermore, because the plastic modulus of this framework is calculated as a function of distance between the current stress point and the conjugated stress point on the bounding surface, it could predict the plastic variation of the water volume fraction, even if the stress point is located within the bounding surface. Therefore, it seems a good choice to simulate problems involving cyclic hydraulic loading, such as drying and wetting paths, by the use of a bounding surface plasticity framework. The bounding surface plasticity framework [48,49] is therefore used for capturing SWCCs. Similar to the LC curve, in relation to the bounding surface framework, the SD and SI yield curves are renamed to the SD and SI bounding curves.

Employing the subloading surface and bounding surface plasticity frameworks in the proposed model is particularly helpful for simulating problems involving multiple cycles of wetting and drying or multiple cycles of mechanical loading and unloading.

Fig. 2 shows the forms of the LC normal yield curve, SI and SD bounding curves and their typical evolution for isotropic stress states. Plastic compression due to mechanical loading causes the LC normal yield curve to move outward. Furthermore, there is a coupling effect on hydraulic behavior. Plastic compression results in a decrease in the dimensions of voids. Therefore, the value of suction will be increased. This phenomenon could be captured by coupled hardening rules, which cause the SI and SD bounding curves to shift upward.

An irrecoverable decrease of the water volume fraction during a drying path causes the upward movement of the SI and SD bound-

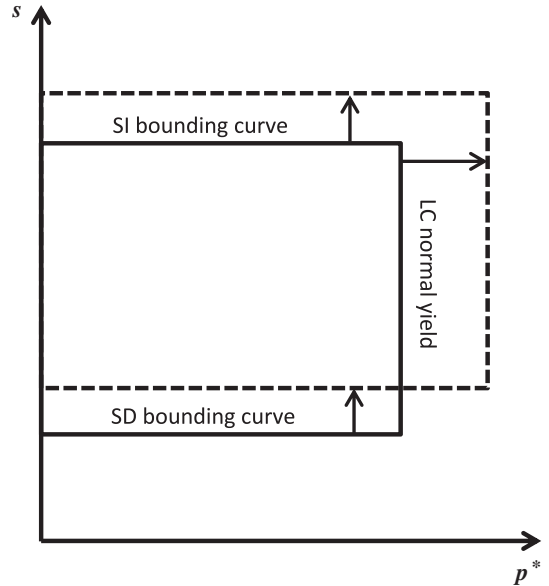


Fig. 2. LC normal yield curve, SI and SD bounding curves and their evolution for isotropic stress state.

ing curves. Similarly during a wetting path, SI and SD bounding curves are shifted downward. Moreover, the plastic evolution of the water volume fraction influences the mechanical behavior of unsaturated soil. The plastic decrease in the value of n_w is produced by voids emptying of water, which is associated with an increase in the number of meniscus water lenses and, thus, a stabilizing of the soil against deformation. This phenomenon will be captured in the model, if the LC normal yield curve moves outward due to a drying path. Similarly, the influence of a plastic increase in the value of n_w due to a wetting path could be simulated with an inward movement of the LC normal yield curve.

Fig. 3 schematically shows a possible extension of the proposed elastoplastic framework to triaxial stress states, with a curved normal yield surface and planar SI and SD bounding surfaces. It should be noted that since suction provides considerable tensile strength to unsaturated soils, the region enclosed by the yield surface should extend to a negative value of p^* . Therefore, the definition of the normal yield surface within the subloading surface elastoplasticity framework, similar to the one proposed by Hashiguchi and Mase [50], is highly recommended.

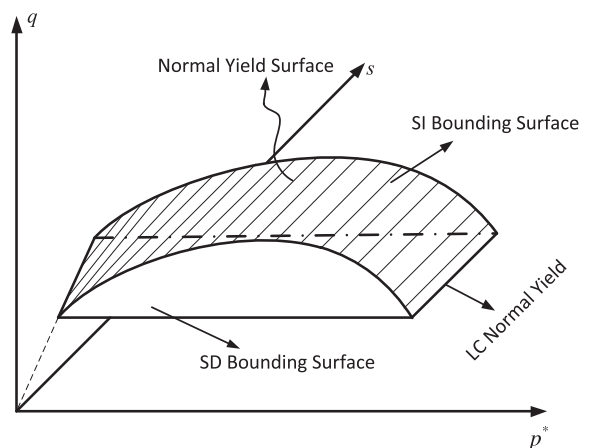


Fig. 3. Schematic of yield surfaces for triaxial stress states.

Using the described framework, the influence of any plastic change in water volume fraction on the stress-strain behavior and the coupling effect on the reverse direction could be simulated by the coupled movement of the LC normal yield curve and the SI and SD bounding curves. This type of coupling between hydraulic and mechanical behavior is derived from the framework proposed by Wheeler et al. [30]. It is worth noting that the coupled movement of bounding curves must be controlled with appropriate coupled hardening rules, which are not clearly and completely described by the existing models.

3. Constitutive model formulation

This section presents the coupled elastoplastic constitutive model for describing the hydro-mechanical behavior of unsaturated soil. As mentioned earlier, the bounding surface and subloading surface frameworks are employed to describe hydraulic and mechanical behavior, respectively. Complete coupling between these two kinds of behavior is achieved by appropriate coupled hardening rules.

3.1. Bounding curves

The normal yield curve and bounding curves are described by the following three functions:

$$p^* = p_0^* \quad (6)$$

$$s = s_{I0} \quad (7)$$

$$s = s_{D0} \quad (8)$$

where p_0^* , s_{I0} and s_{D0} introduce the position of the LC normal yield curve and SI and SD bounding curves, respectively. The initial value of p_0^* depends on the maximum pressure experienced by the soil and must be introduced as a calibration parameter. The evolution of p_0^* will be controlled by coupled hardening rules, which will be introduced later.

Based on Muraleetharan et al. [33] and Liu and Muraleetharan [46], the initial values and evolution rules of s_{D0} and s_{I0} are described with primary wetting and secondary drying curves, respectively. They observed that all scanning curves are bounded by these two curves. If the soil starts from an oven dried state and is then subjected to wetting, it will follow the primary wetting curve. If wetting is continued until the saturated state, and is then subjected to drying, the soil will follow the secondary drying curve. These two curves are presented in Fig. 4 and can be described mathematically by the equations proposed by Feng and Fredlund [51]:

$$s_{D0} = b_1 \times \left[\frac{n_{wsat} - n_w}{n_w - n_{wres}} \right]^{\frac{1}{d_1}} \quad (9)$$

$$s_{I0} = b_2 \times \left[\frac{n_{wsat} - n_w}{n_w - n_{wres}} \right]^{\frac{1}{d_2}} \quad (10)$$

where n_{wsat} is the value of the water volume fraction at zero suction, n_{wres} is value of the water volume fraction at a very high suction, and b_1 , d_1 , b_2 and d_2 are four material parameters that describe the primary wetting and secondary drying curves in the $s:n_w$ plane. The initial values of s_{D0} and s_{I0} can be calculated using Eqs. (9) and (10) and applying an initial value of n_w .

3.2. Coupled hardening rules

As described in the last section, plastic compression during loading causes the LC normal yield curve to move outward. Addi-

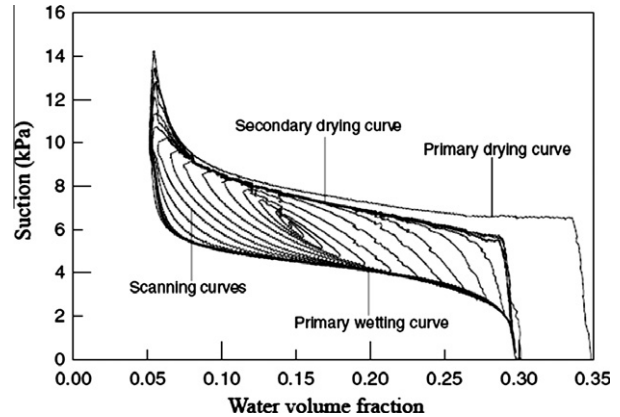


Fig. 4. Example of soil water characteristic curves [33].

tionally, both a plastic decrease and increase of the water volume fraction cause the LC normal yield curve to move outward and inward, respectively. This behavior can be represented by the following hardening rule [33]:

$$dp_0^* = k_0 d\epsilon_v^p - k_1 dn_w^p \quad (11)$$

k_0 and k_1 in this equation are introduced as follows:

$$k_0 = p_0^* \eta_0 v \quad (12)$$

$$k_1 = p_0^* \eta_1 \quad (13)$$

where v is the specific volume and η_0 and η_1 are two material parameters which control the movement of LC yield curve due to plastic volumetric strain and plastic change of water volume fraction, respectively. It is worth noting that the specific volume can be defined in terms of porosity (n):

$$v = \frac{1}{1-n} \quad (14)$$

and its variation during the analysis could be calculated as;

$$dv = \frac{n d\epsilon_v - d\epsilon_v^p}{(1-n)^2} \quad (15)$$

Commonly in the theory of soil plasticity, it is assumed that the elastic part of mechanical strain attributes to deformation of solid grains, and its plastic part attributes to deformation of voids due to slippage at inter-particle or inter-packet contacts. In addition, due to very small compressibility factor of solid grains, sizes of voids could be assumed to be only influenced by the plastic part of mechanical deformation.

The plastic part of compression and expansion causes the primary wetting and secondary drying curves to move right and left in the $s:n_w$ plane. Fig. 5 shows the possible movement of primary wetting and secondary drying curves due to compression. This phenomenon can be captured in the model by altering the value of n_{wsat} and n_{wres} using the appropriate evolution rules. The initial values of n_{wsat} and n_{wres} are considered as material parameters and their evolution rules are described below:

$$dn_{wres} = \alpha_1 n_w d\epsilon_v^p \quad (16)$$

$$dn_{wsat} = \alpha_2 n_w d\epsilon_v^p \quad (17)$$

where α_1 and α_2 are two material parameters which control the movement of primary wetting and secondary drying curves due to plastic volumetric strain. It should be noted that with respect

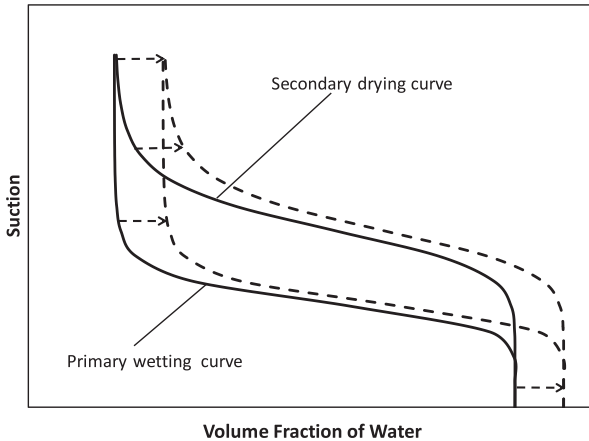


Fig. 5. Movement of primary wetting and secondary drying curves due to plastic part of volumetric deformation.

to Eqs. (9), (10), (16), and (17), movement of SI and SD bounding curves is defined as a function of the plastic volumetric strain in addition to the water volume fraction.

The movement of the SD and SI bounding curves can be controlled using the primary wetting and secondary drying curves. Because the values of s_{D0} and s_{I0} must always lie on the primary wetting and secondary drying curves, the hardening rules of SD and SI bounding curves can be obtained by differentiating Eqs. (9) and (10). The coupled hardening rules are defined as below:

$$ds_{D0} = \frac{\partial s_{D0}}{\partial n_w^p} dn_w^p + \frac{\partial s_{D0}}{\partial \varepsilon_v^p} d\varepsilon_v^p \quad (18)$$

$$ds_{I0} = \frac{\partial s_{I0}}{\partial n_w^p} dn_w^p + \frac{\partial s_{I0}}{\partial \varepsilon_v^p} d\varepsilon_v^p \quad (19)$$

3.3. Elastoplastic calculations

The elastic evolution of the water volume fraction and the volumetric strain are described as follows:

$$d\varepsilon_v^e = \frac{kdp^*}{vp^*} \quad (20)$$

$$dn_w^e = \frac{ds}{\Gamma^e} \quad (21)$$

where k stands for the slope of the elastic swelling line in the $v: \ln p^*$ plane, and Γ^e is the elastic capillary modulus.

The evolution of the plastic volumetric strain is calculated as:

$$d\varepsilon_v^p = \frac{dp^*}{K^p} \quad (22)$$

where K^p can be calculated in the framework of the subloading surface plasticity as below:

$$K^p = \left(\frac{1}{p_0^*} + \frac{U}{R} \right) p^* \quad (23)$$

The parameter R is defined as the ratio of the distance between the current stress point and a specific reference, and the distance between its conjugated stress point on the normal yield surface and the same reference. In the proposed model this parameter is equal to $\frac{p^*}{p_D^*}$ as shown in Fig. 6, and U is the monotonically decreasing function of R that satisfies the following conditions:

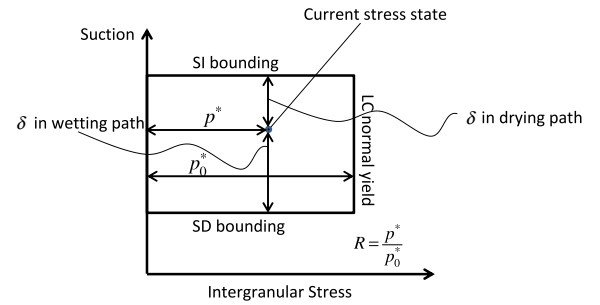


Fig. 6. Graphical representation of δ and R .

$$\begin{aligned} U &= \infty \text{ for } R = 0 \\ U &> 0 \text{ for } 0 < R < 1 \\ U &= 0 \text{ for } R = 1 \\ U &< 0 \text{ for } R > 1 \end{aligned} \quad (24)$$

These conditions are required to guarantee that the stress state approaches the LC normal yield curve during the loading process even if it goes out from the normal yield state ($R > 1$) [44]. It is worth noting that although the situation $R > 1$ is physically meaningless, it might be occurred during a rough numerical calculation with large loading steps. Consequently numerical code, which used conventional plasticity frameworks, should provide special numerical techniques in order that the stress point does not deviate from the yield surface in the plastic loading process. Nevertheless, the function satisfying conditions (24) is introduced by Hashiguchi [52] as:

$$U = -u \ln R \quad (25)$$

where u is a material parameter. The loading criterion for volumetric strain is given as follows:

$$\begin{cases} \frac{k}{vp^*} d\varepsilon_v > 0 \rightarrow d\varepsilon_v^p \neq 0 \\ \frac{k}{vp^*} d\varepsilon_v \leqslant 0 \rightarrow d\varepsilon_v^p = 0 \end{cases} \quad (26)$$

Note that Eq. (26) is derived from the loading criterion proposed by Hashiguchi [53].

The variation of the suction and water volume fraction are reflected in dp^* , expressed as:

$$dp^* = dp_{net} + n_w ds + sd n_w \quad (27)$$

This means that, Eq. (22) includes the coupling effects of the water volume fraction on volumetric deformation in addition to any direct effects of mechanical loading. By differentiating the equation that defines the volume fraction of water ($n_w = \frac{v_w}{v}$), the increment of n_w can be given as:

$$dn_w = \frac{dv_w}{v} + n_w d\varepsilon_v \quad (28)$$

where v_w and v are the volume of water and total volume of medium, respectively. Eq. (28) shows that, any change in the value of the water volume fraction (dn_w) is the result of variation in the volume of water (dv_w) and variation in the volume of the porous medium ($d\varepsilon_v$). Similarly, the plastic part of the water volume fraction increment (dn_w^p) is the result of plastic variation in the volume of water (dv_w^p) and plastic variation in the volume of the porous medium ($d\varepsilon_v^p$). In the proposed model, any plastic change in the volume of water is calculated based on the variation in matric suction. Moreover, the plastic part of the volumetric strain is calculated by the use of Eq. (22). Thus, the plastic part of the water volume fraction is calculated as below:

$$dn_w^p = \frac{dv_w^p}{v} + n_w d\varepsilon_v^p = \frac{ds}{\Gamma^p} + n_w \frac{dp^*}{K^p} \quad (29)$$

where Γ^p is the plastic capillary modulus, which can be calculated in the bounding surface elastoplasticity framework [33]:

$$\Gamma^p = \Gamma_0^p \left(1 + h \cdot \frac{\delta}{\langle \delta_{in} - g\delta \rangle} \right) \quad (30)$$

where h and g are two material parameters; $\langle \rangle$ are Macaulay brackets; δ is the distance of current stress state to the SD or SI bounding curves in the wetting or drying process, respectively (Fig. 6); δ_{in} is the value of δ at the beginning of each wetting/drying path, and Γ_0^p is the value of Γ^p on the SD or SI bounding curves in the wetting or drying process, respectively. The value of Γ_0^p is calculated as:

$$\Gamma_0^p = \frac{ds_{D0}}{dn_w} \quad \text{in wetting path} \quad (31)$$

$$\Gamma_0^p = \frac{ds_{J0}}{dn_w} \quad \text{in drying path} \quad (32)$$

Eq. (30) indicates that if $\delta = \delta_{in}$ then $\Gamma^p = \infty$, it means elastic behavior dominates, which is the case at the beginning of each wetting or drying path. If $\delta = 0$ then $\Gamma^p = \Gamma_0^p$, it means the stress state lies on the corresponding bounding curve.

It should be noted, the shape of the scanning curves in the proposed model is considered similar to the bounding curves unless it is flatter. It means that if drying is halted partway down the secondary drying curve and wetting is started, the soil will follow an intermediate scanning curve, which is flatter than the primary wetting curve, until the primary wetting curve is reached. Similarly, if wetting is halted partway up the primary wetting curve and drying is started, the soil will follow another scanning curve, which is flatter than the secondary drying curve, until the secondary drying curve is reached. The parameters Γ^e , h and g control the behavior of these scanning curves.

4. Comparisons with experiments

To examine the ability of the proposed model to simulate the real behavior of unsaturated soil in an acceptable way, experimental results using Pearl clay [54] and a bentonite–kaolin mixture [28] are compared with model predictions.

Pearl clay behaves like collapsible soil. Collapsible soil consists of loose materials that collapses and compacts under the addition of water or excessive loading. By contrast, bentonite–kaolin mixtures behave as highly expansive soils. Expansive soil consists of clayey materials that notably shrinks and swells due to drying and wetting paths, respectively.

Expansive and collapsible soils are geological hazards that are widely distributed around the world. These soils experience notable volumetric deformation in response to wetting and drying, often resulting in considerable damage to structures. Hydro-mechanical simulation of collapsible and expansive soils is a subject of great interest in geotechnical engineering practice. Expansive and collapsible soils behave conversely due to their responses to wetting and drying paths. Modeling these types of behaviors in unified constitutive equations is one of the abilities of the proposed model.

It is worth noting that the stress paths applied to the test samples are introduced in terms of mean net stress (p_{net}) and suction (s). Since an increment of p^* (Eq. (25)) involves dn_w , it has to be solved simultaneously with the constitutive model equations before the stress path can be defined in the $p^*:s$ plane.

4.1. Determination of parameters

The proposed model requires nine parameters to describe hydraulic behavior, four parameters to describe stress-strain

behavior and three parameters to account for coupling effects. The secondary drying curve, the primary wetting curve and a scanning curve are required to determine the retention parameters ($b_1, d_1, b_2, d_2, \Gamma^e, h, g, n_{w_{sat}}, n_{w_{res}}$). The values of $n_{w_{sat}}$ and $n_{w_{res}}$ can be determined from the maximum and minimum value of n_w at the primary wetting and secondary drying curves, respectively. The values of b_1, d_1 and b_2, d_2 can be determined by conducting a curve-fitting procedure on primary wetting and secondary drying curves using Eqs. (9) and (10), respectively. The values of Γ^e, h and g may be found by a trial-and-error procedure using the scanning curve data from laboratory tests. Then, the results of an isotropic compression test with wetting or drying and loading–unloading processes are required to calibrate the stress–strain and coupling parameters ($p_0^*, u, k, \eta_0, \eta_1, \alpha_1, \alpha_2$). The initial value p_0^* can be determined as the yielding point of the results plotted in the $p^*:v$ plane. The parameters u and η_0 are determined by fitting the curvature and slope of the stress–strain diagram in the $\ln p^*:v$ plane, respectively. It should be noted that the proposed model provides the possibility of predicting nonlinear curves in $\ln p^*:v$ plane by combining these two parameters. This type of behavior is usually observed in highly expansive soils. The parameter k stands for the slope of the elastic swelling line in the $\ln p^*:v$ plane. The coupling parameter η_1 can be found by fitting the diagram of soil behavior in $s-v$ plane. The remains coupling parameters α_1 and α_2 can be found by a trial-and-error procedure to fit the diagram of soil behavior in p^*-n_w plane. It is worth noting that since the specific volume varies during the experimental measurement of SWCCs, the initial values of $n_{w_{sat}}$ and $n_{w_{res}}$, which are determined by the maximum and minimum value of n_w at the primary wetting and secondary drying curves, do not correspond to the initial specific volume. Therefore, in order to accurately reproduce the primary wetting and secondary drying curves, some modifications on the initial values of $n_{w_{sat}}$ and $n_{w_{res}}$ are required to fit the computed curves with those obtained by laboratory.

Alternatively, if the primary wetting and secondary drying and scanning curves are not available (e.g., Section 4.3), the parameters can be found by a trial-and-error procedure using the mean net stress versus specific volume data, the mean net stress versus degree of saturation data, suction versus degree of saturation data and suction versus specific volume data coming from an isotropic compression test with wetting–drying and loading–unloading processes.

4.2. Pearl clay (collapsible soil)

In this section, the comparison results of model predictions and of test data using Pearl clay are presented. The Pearl clay, which

Table 1
Constitutive model parameters for the Pearl clay.

SWCCs parameters	
b_1	22 kPa
d_1	1.635
b_2	105 kPa
d_2	4.8
Γ^e	-9000 kPa
h	10
g	0.1
$n_{w_{sat}}$	0.57
$n_{w_{res}}$	0.305
Mechanical parameters	
p_0^*	113 kPa
u	225
η_0	17.5
k	0.07
Coupling parameters	
η_1	10
α_1	0.1
α_2	0.1

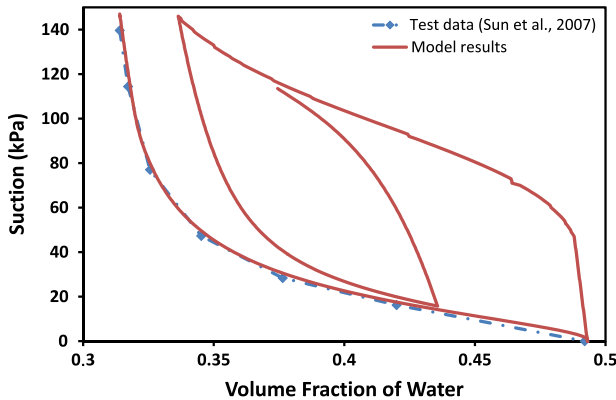


Fig. 7. Comparison between the measured and predicted SWCCs for Pearl clay.

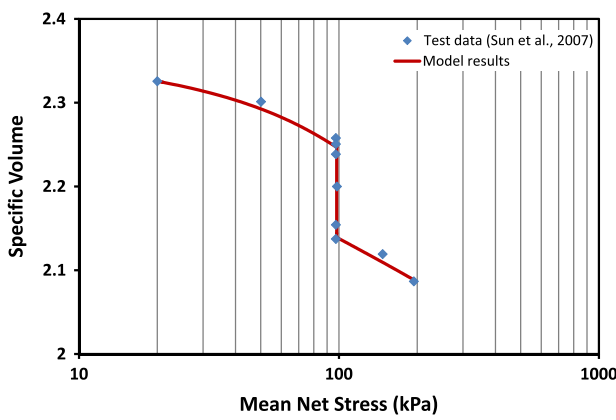


Fig. 8. Comparison between the measured and predicted results of collapse test for Pearl clay: wetting at a mean net stress of 98 kPa.

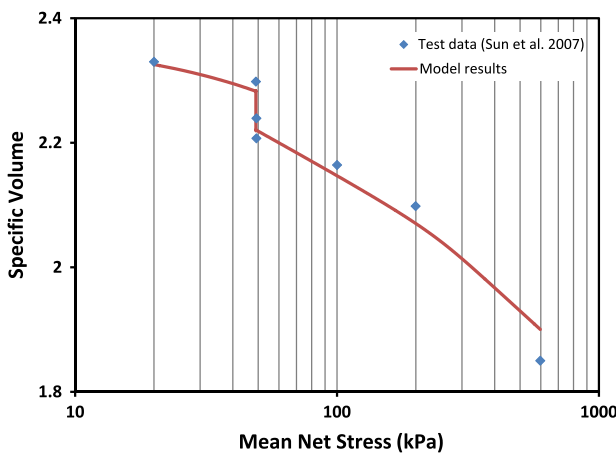


Fig. 9. Comparison between the measured and predicted results of collapse test for Pearl clay: wetting at a mean net stress of 49 kPa.

was used by Sun et al. [54], had a liquid limit of 49, a plasticity index of 22 and a specific gravity of 2.71. The material parameters that are used to predict the soil behavior are listed in Table 1.

Fig. 7 shows a comparison of test data and model predictions for a wetting path. The value of n_w and n at the beginning of the test are 0.314 and 0.57, respectively. It should be noted that these initial values are determined directly from the conditions reported by the laboratory. The value of the mean net stress is kept constant at 20 kPa during the test. The value of suction is equal to 147 kPa at

Table 2

Constitutive model parameters for the bentonite–kaolin mixture.

<i>SWCCs parameters</i>	
b_1	36 kPa
d_1	3
b_2	1135 kPa
d_2	0.77
Γ^e	-20,000 kPa
h	30
g	1.3
$n_{w_{sat}}$	0.5
$n_{w_{res}}$	0.17
<i>Mechanical parameters</i>	
p_0^*	157 kPa
u	50
η_0	4.5
k	0.047
<i>Coupling parameters</i>	
η_1	8.5
α_1	1.0
α_2	0.1

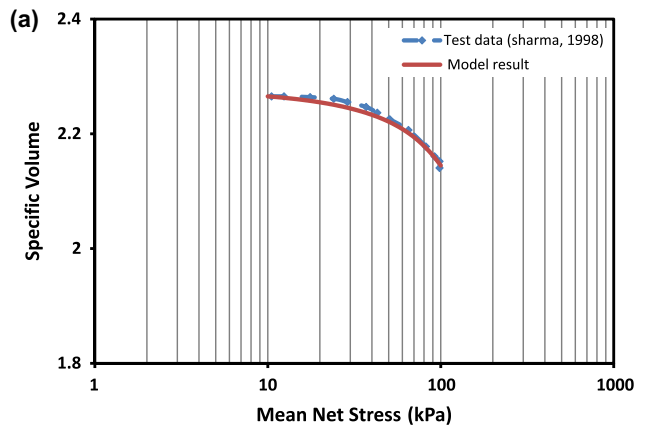


Fig. 10. Comparison between the measured and predicted results for bentonite–kaolin mixture under mechanical loading: (a) specific volume and (b) degree of saturation.

the beginning of the test and decreases to zero due to the wetting process. As shown in the figure, the test data are only available for the first wetting path. However, the model prediction for two cycles of wetting and drying paths is shown in Fig. 7 to represent the ability of the model to simulate hydraulic hysteresis.

Fig. 8 shows the test results and model predictions for a one-dimensional collapse test on Pearl clay. The initial conditions for this test are the same as for the previous test. The stress path for this test involved three different phases:

Phase 1 : Constant suction = 147 kPa mean net stress
 $= 20 \text{ kPa} \rightarrow 98 \text{ kPa}$

Phase 2 : Constant mean net stress = 98 kPa suction
 $= 147 \text{ kPa} \rightarrow 0 \text{ kPa}$

Phase 3 : Constant suction = 0 kPa mean net stress = 98 kPa
 $\rightarrow 196 \text{ kPa}$

Fig. 9 shows the comparison of test data and model results for another collapse test on Pearl clay. The initial conditions for this test are the same as for the previous test. The loading phases of this test are:

Phase 1 : Constant suction = 147 kPa mean net stress
 $= 20 \text{ kPa} \rightarrow 49 \text{ kPa}$

Phase 2 : Constant mean net stress = 49 kPa suction
 $= 147 \text{ kPa} \rightarrow 0 \text{ kPa}$

Phase 3 : Constant suction = 0 kPa mean net stress = 49 kPa
 $\rightarrow 597 \text{ kPa}$

Results of the collapse tests on Pearl clay show the occurrence of plastic compression during the wetting path. This phenomenon is simulated by the proposed model reasonably well compared with the measured results (**Figs. 8 and 9**). It is worth noting that plastic compression during the wetting path occurs in the collapsible soil.

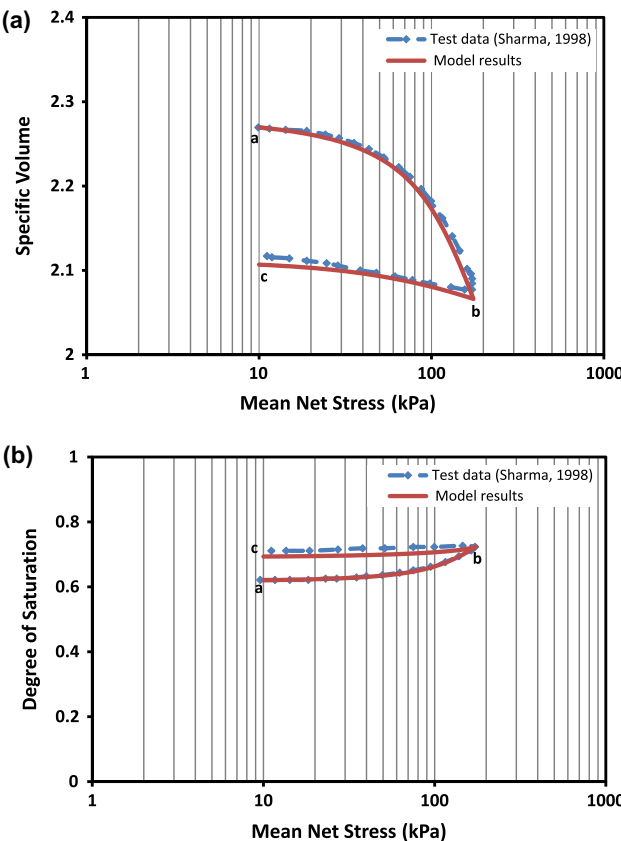


Fig. 9. Comparison between the measured and predicted results for Pearl clay under three loading phases: (a) specific volume and (b) degree of saturation.

4.3. Bentonite–kaolin mixture (highly expansive soil)

Sharma [28] reported the hydro-mechanical behavior of bentonite–kaolin mixture for a mix of 10% Wyoming sodium bentonite and 90% speswhite kaolin. The mixture, which was prepared and used for tests, had a liquid limit of 93, a plastic index of 33 and a dry density of 1.24 Mg/m³. The material parameters that are used to predict the soil behavior are listed in **Table 2**.

Fig. 10 shows the test results and model predictions for a single isotropic loading stage on a bentonite–kaolin mixture in a triaxial cell. The values of n_w and n at the beginning of the test are 0.365 and 0.56, respectively. In the loading stage, the mean net stress increased from 10 kPa to 100 kPa, with a constant suction value of 200 kPa. Variation of the specific volume and degree of saturation in response to the applied mechanical stresses are shown in **Fig. 10** and reasonable agreement is achieved.

Fig. 11 shows the comparison of test data and model predictions for mechanical loading and unloading stages. The initial values of n_w and n for this test are 0.347 and 0.56, respectively. Mechanical loading and unloading are applied under a constant suction of 300 kPa. The mean net stress increased from 10 kPa to 175 kPa and then decreased to 10 kPa. The test data show the influence of plastic volumetric strain on the value of water saturation, which appears in **Fig. 11b** as the occurrence of irreversible change in water saturation due to the mechanical loading and unloading stages (Points a and c are not coincident). This coupling effect is captured by the proposed model reasonably well.

Fig. 12 shows the test results and model predictions for wetting and drying cycles. The values of n_w and n at the beginning of the test are 0.338 and 0.56, respectively. Wetting and drying cycle are achieved by decreasing the suction value from 300 kPa to

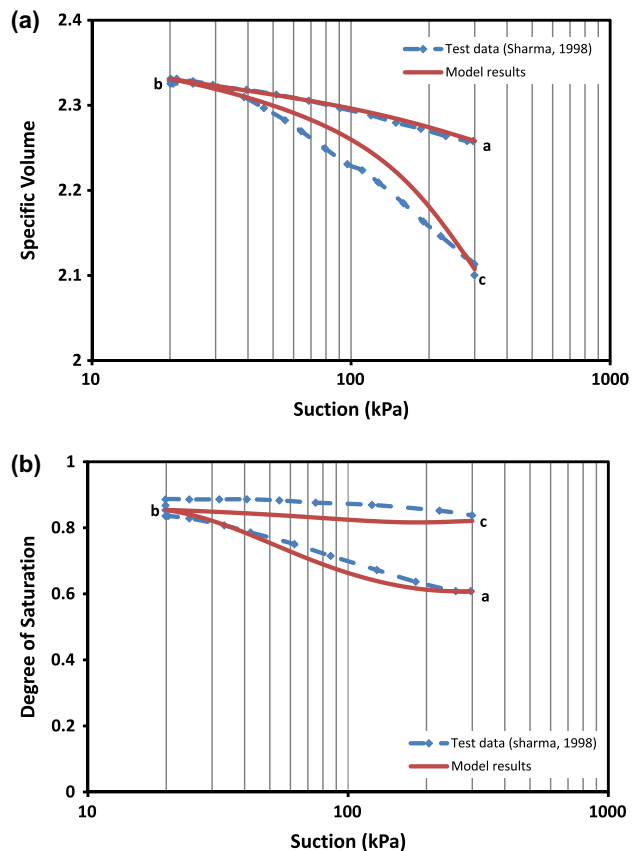


Fig. 11. Comparison between the measured and predicted results for bentonite–kaolin mixture under mechanical loading and unloading: (a) specific volume and (b) degree of saturation.

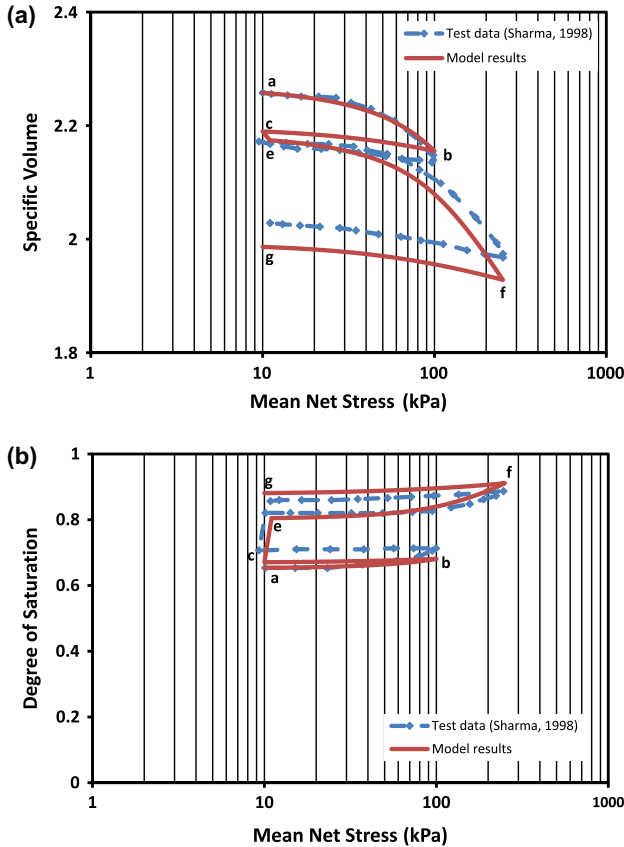


Fig. 13. Comparison between the measured and predicted results for bentonite-kaolin mixture under mechanical loading/unloading and wetting/drying cycle: (a) specific volume and (b) degree of saturation.

10 kPa and then increasing it from 10 kPa to 300 kPa. The mean net stress is kept constant during the test. Fig. 12a shows the occurrence of plastic volumetric strain due to the wetting and drying stages. In the wetting path a–b, the soil swells but then notably greater compression occurs during the subsequent drying path b–c. Fig. 12b shows the occurrence of hydraulic hysteresis. The value of the degree of saturation during the drying path is higher than the wetting path. These phenomena are also captured reasonably well in the proposed model.

Fig. 13 shows the test and model results for mechanical loading and unloading and wetting and drying cycles. The initial values of n_w and n are 0.36 and 0.56, respectively. The stress path for this test involved three different phases as follows:

Phase 1 : Constant suction = 200 kPa mean net stress

$$= 10 \text{ kPa} \rightarrow 100 \text{ kPa} \rightarrow 10 \text{ kPa}$$

Phase 2 : Constant mean net stress = 10 kPa suction

$$= 200 \text{ kPa} \rightarrow 50 \text{ kPa} \rightarrow 200 \text{ kPa}$$

Phase 3 : Constant suction = 200 kPa mean net stress

$$= 10 \text{ kPa} \rightarrow 250 \text{ kPa} \rightarrow 10 \text{ kPa}$$

Fig. 13a shows no irreversible compression occurred during the drying path (Points c and e are almost coincident in the test data). Meanwhile, the model predicts a slight compression due to the coupling effects of water saturation on volumetric strain. Fig. 13b shows a significant increase in the degree of saturation during the wetting and drying cycle c–d–e (loading phase 2, which is

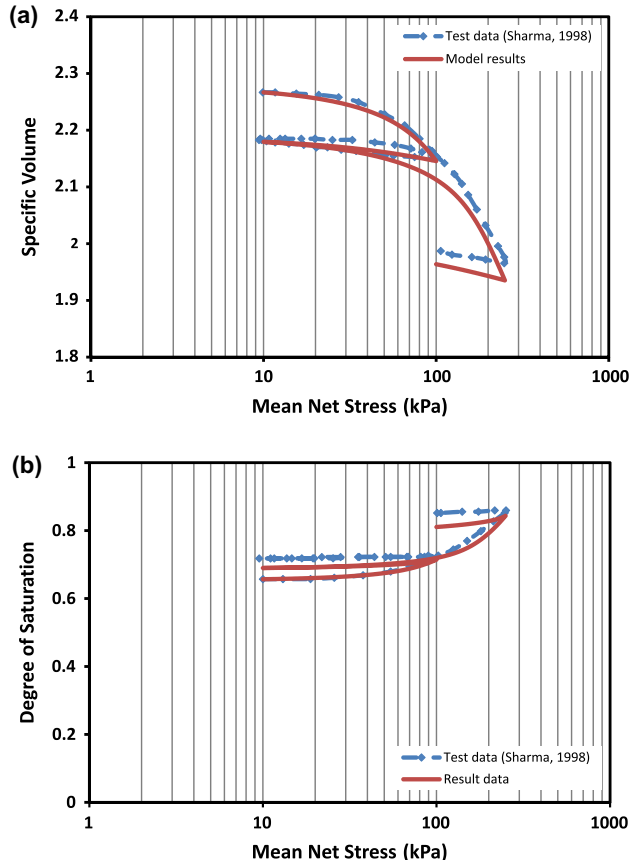


Fig. 14. Comparison between the measured and predicted results for bentonite-kaolin mixture under multiple cycles of mechanical loading and unloading: (a) specific volume and (b) degree of saturation.

not shown in the figure) as a consequence of hydraulic hysteresis. During the second mechanical loading stage (e–f–g path), the yielding point of the curve occurred at a mean net stress lower than the 100 kPa previously applied. These phenomena are predicted reasonably well by the proposed model.

The test data and model results for two cycles of mechanical loading and unloading ($p_{net} = 10 \text{ kPa} \rightarrow 100 \text{ kPa} \rightarrow 10 \text{ kPa} \rightarrow 250 \text{ kPa} \rightarrow 100 \text{ kPa}$) are shown in Fig. 14. The initial conditions of this test are the same as for the previous test. The mechanical loading and unloading stages are performed at the constant value of suction equal to 200 kPa. Fig. 14b shows that a significant change of degree of saturation occurred, although the suction was held constant. This phenomenon shows the influence of plastic volumetric strain on the variation of degree of saturation, which is predicted reasonably well by the proposed model.

5. Concluding remarks

A review of the main characteristics of unsaturated soil behavior has shown that coupling of hydraulic and mechanical behavior is one of the main difficulties for existing models. In this paper, a new elastoplastic constitutive model for isotropic loading conditions is developed that assesses the coupling of hydraulic and mechanical behavior in unsaturated soil more completely than existing models. This model is proposed in the framework of two stress-state variables. The employed stress variables are intergranular stress and matric suction, which are conjugated with the conventional strain increment and the decrement of the water volume fraction, respectively.

The occurrence of plastic compression and expansion due to wetting and drying paths are captured in the proposed model implicitly by employing the intergranular stress. However, the plastic evolution of water volume fraction due to mechanical loading is considered explicitly in the constitutive formulation. Furthermore, to achieve a better description of coupled hydro-mechanical behavior, the influence of plastic deformation on the position of primary wetting and secondary drying curves (bounding curves) is considered by applying some coupled hardening rules.

In the proposed model, subloading surface and bounding surface plasticity frameworks are employed to describe the mechanical and hydraulic behavior, respectively. Because there are no purely elastic domains in the selected frameworks, the proposed model fulfills the smoothness condition, and thus, the smooth elastic-plastic transition is described.

The proposed model provides a realistic representation of hydraulic and mechanical behavior, which is an essential requirement for numerical modeling of coupled hydro-mechanical problems. It is applied to predict the hydro-mechanical behavior of Pearl clay (as a collapsible soil) and bentonite-kaolin mixture (as an expansive soil), and thus, the ability of model has been verified.

It should be noted, although several models can simulate the behavior of Pearl clays, but not all models can reproduce accurately the behavior of bentonite-kaolin mixture. Modeling these types of behaviors in unified constitutive equations could be mentioned as the superiority of the proposed model in comparison with previous ones.

References

- [1] Hoxha D, Girauda A, Homanda F, Auvray C. Saturated and unsaturated behavior modelling of Meuse-Haute/Marne argillite. *Int J Plast* 2007;23(5):733–66.
- [2] Coussy O, Pereira J, Vaunat J. Revisiting the thermodynamics of hardening plasticity for unsaturated soils. *Comput Geotech* 2010;37(1–2):207–15.
- [3] Zhao C, Liu Y, Gao F. Work and energy equations and principle of generalized effective stress for unsaturated soils. *Int J Numer Anal Methods Geomech* 2010;34:920–36.
- [4] Bishop A. The principle of effective stress. *Tek UKEBL* 1959;106(39):113–43.
- [5] Blight G. Strength and consolidation characteristics of compacted soils. PhD dissertation, University of London, London; 1961.
- [6] Doland I. The mechanical properties of saturated and partly saturated soils with special reference to negative pore water pressure. PhD dissertation, University of London, London; 1961.
- [7] Jennings J, Burland J. Limitations to the use of effective stresses in partly saturated soils. *Geotechnique* 1962;12(2):125–44.
- [8] Coleman J. Stress/Strain relations for partly saturated soils. *Geotechnique* 1962;12(4):348–50.
- [9] Bishop A, Blight G. Some aspects of effective stress in saturated and unsaturated soils. *Geotechnique* 1963;13(3):177–97.
- [10] Blight G. A study of effective stress for volume change. In: Moisture equilibria and moisture changes in soils beneath covered. Sydney: Butterworth; 1965. p. 256–69.
- [11] Fredlund D, Morgenstern N. Stress state variables for unsaturated soils. *J Geotech Eng Div* 1977;103(5):447–66.
- [12] Kohgo Y, Nakano M, Miyazaki T. Theoretical aspects of constitutive modelling for unsaturated soils. *Soil Found* 1993;33(4):49–63.
- [13] Bolzon G, Schrefler B, Zienkiewicz O. Elastoplastic soil constitutive laws generalised to partially saturated states. *Geotechnique* 1996;46(2):270–89.
- [14] Loret B, Khalili N. A three-phase model for unsaturated soil. *Int J Numer Anal Methods Geomech* 2000;24:893–927.
- [15] Khalili N, Loret B. An elasto-plastic model for nonisothermal analysis of flow and deformation in unsaturated soils: formulation. *Int J Solids Struct* 2001;38:8305–30.
- [16] Khalili N, Geiser F, Blight G. Effective stress in unsaturated soils: review with new evidence. *Int J Geomech* 2004;4(2):115–26.
- [17] Nuth M, Laloui L. Effective stress concept in unsaturated soils: clarification and validation of a unified framework. *Int J Numer Anal Methods Geomech* 2008;32:771–801.
- [18] Laloui L, Nuth M. On the use of the generalised effective stress in the constitutive modelling of unsaturated soils. *Comput Geotech* 2009;36(1–2):20–3.
- [19] Vlahinic I, Jennings H, Andrade J, Thomas J. A novel and general form of effective stress in a partially saturated porous material: the influence of microstructure. *Mech Mater* 2011;43:25–35.
- [20] Alonso E, Gens A, Josa A. A constitutive model for partially saturated soils. *Geotechnique* 1990;40(3):405–30.
- [21] Gens A. Constitutive laws. In: Gens A, Jouanna P, Schrefler BA, editors. Modern issues in nonsaturated soils. Wien: Springer-Verlag; 1995. p. 129–58.
- [22] Wheeler S, Sivakumar V. An elasto-plastic critical state framework for unsaturated soil. *Geotechnique* 1995;45(1):35–53.
- [23] Cui Y, Delage P. Yielding and plastic behaviour of an unsaturated compacted silt. *Geotechnique* 1996;46(2):291–311.
- [24] Sanchez M, Gens A, Guimaraes L, Olivella S. A double structure generalized plasticity model for expansive materials. *Int J Numer Anal Methods Geomech* 2005;29:751–87.
- [25] Gallipoli D, Gens A, Sharma R, Vaunat J. An elasto-plastic model for unsaturated soil incorporating the effects of suction and degree of saturation on mechanical behaviour. *Geotechnique* 2003;53(1):123–35.
- [26] Fredlund D, Rahardjo H. Soil mechanics for unsaturated soils. New York: John Wiley and Sons; 1993.
- [27] Wheeler S. Inclusion of specific water volume within an elasto-plastic model for unsaturated soils. *Can Geotech J* 1996;33:42–57.
- [28] Sharma R. Mechanical behavior of unsaturated highly expansive clays. PhD dissertation, University of Oxford, UK; 1998.
- [29] Sun D, Sun W, Xiang L. Effect of degree of saturation on mechanical behaviour of unsaturated soils and its elastoplastic simulation. *Comput Geotech* 2010;37(5):678–88.
- [30] Wheeler S, Sharma R, Buisson M. Coupling of hydraulic hysteresis and stress-strain behavior in unsaturated soils. *Geotechnique* 2003;53(1):41–53.
- [31] Sheng D, Sloan S, Gens A. A constitutive model for unsaturated soils: thermomechanical and computational aspects. *Comput Mech* 2004;33:453–65.
- [32] Sun D, Sheng D, Sloan S. Elastoplastic modelling of hydraulic and stress-strain behaviour of unsaturated soils. *Mech Mater* 2007;39:212–21.
- [33] Muraleetharan K, Liu C, Wei C, Kibbey T, Chen L. An elastoplastic framework for coupling hydraulic and mechanical behavior of unsaturated soils. *Int J Plast* 2009;25(3):473–90.
- [34] Masin D. Predicting the dependency of a degree of saturation on void ratio and suction using effective stress principle for unsaturated soils. *Int J Numer Anal Methods Geomech* 2010;34:73–90.
- [35] D'Onza F, Gallipoli D, Wheeler S, Casini F, Vaunat J, Khalili N, et al. Benchmarking different approaches to constitutive modelling of unsaturated soils. *Geotechnique* 2010;61(4):283–302.
- [36] Sheng D. Review of fundamental principles in modeling unsaturated soil behavior. *Comput Geotech* 2001;38(6):757–76.
- [37] Dafalias Y, Popov E. A model of nonlinearly hardening materials for complex loading. *Acta Mech* 1975;21:173–92.
- [38] Dafalias Y, Popov E. Plastic internal variables formalism of cyclic plasticity. *ASME J Appl Mech* 1976;43:645–51.
- [39] Khalili N, Habte M, Zargarbashi S. A fully coupled flow deformation model for cyclic analysis of unsaturated soils including hydraulic and mechanical hysterese. *Comput Geotech* 2008;35(6):872–89.
- [40] Wei C. Static and dynamic behavior of multiphase porous media: Governing equations and finite element implementation. PhD dissertation, University of Oklahoma, Oklahoma; 2001.
- [41] Hashiguchi K. Subloading surface model in unconventional plasticity. *Int J Solids Struct* 1989;25(8):917–45.
- [42] Hashiguchi K, Saitoh K, Okayasu T, Tsutsumi S. Evaluation of typical conventional and unconventional plasticity models for prediction of softening behaviour of soils. *Geotechnique* 2002;52(8):561–78.
- [43] Hashiguchi K. Fundamental requirements and formulation of elastoplastic constitutive equations with tangential plasticity. *Int J Plast* 1993;9:525–49.
- [44] Hashiguchi K. Mechanical requirements and structures of cyclic plasticity models. *Int J Plast* 1993;9:721–48.
- [45] Li X. Modelling of hysteresis response for arbitrary wetting/drying paths. *Comput Geotech* 2005;32:133–7.
- [46] Liu C, Muraleetharan K. Description of soil water characteristic curves using the bounding surface plasticity theory. In: 4th international conference on unsaturated soils; 2006. p. 2432–40.
- [47] Kohgo Y. A hysteresis model of soil water retention curves based on bounding surface concept. *Soil Found* 2008;48(5):633–40.
- [48] Dafalias Y, Herrmann L. A bounding surface soil plasticity model. In: Proceeding of international symposium on soils under cyclic and transient loading, Swansea; 1980. p. 335–45.
- [49] Dafalias Y, Herrmann L. Bounding surface formulation of plasticity. In: Pande G, Zienkiewicz O, editors. Soil mechanics – transient and cyclic loads; 1982. p. 253–82.
- [50] Hashiguchi K, Mase T. Extended yield condition of soils with tensile yield strength and rotational hardening. *Int J Plast* 2007;23(12):1939–56.
- [51] Feng M, Fredlund D. Hysteretic influence associated with thermal conductivity sensor measurements. In: Proceeding of from theory to the practice of unsaturated soil mechanics, in associated with 52nd Can. Geotech. conference and unsaturated soil group, Regiana; 1999. p. 14:2:14–14:2:20.
- [52] Hashiguchi K. Constitutive equations of elastoplastic materials with elastic-plastic transition. *J Appl Mech* 1980;47(2):266–72.
- [53] Hashiguchi K. On the loading criterion. *Int J Plast* 1994;10(8):871–8.
- [54] Sun D, Sheng D, Xu Y. Collapse behavior of unsaturated compacted soil with different initial densities. *Can Geotech J* 2007;44:673–86.